



**Probing the coupling of butterfly wing photonic crystals to
plasmon resonances with surface-enhanced Raman
spectroscopy**

Journal:	<i>Journal of Materials Chemistry C</i>
Manuscript ID	TC-ART-05-2019-002629.R2
Article Type:	Paper
Date Submitted by the Author:	17-Oct-2019
Complete List of Authors:	Palmer, Levi; University of Minnesota, Chemistry Brooks, James; University of Minnesota, Chemistry Frontiera, Renee; University of Minnesota, Chemistry

SCHOLARONE™
Manuscripts

Probing the coupling of butterfly wing photonic crystals to plasmon resonances with surface-enhanced Raman spectroscopy

Levi D. Palmer, James L. Brooks, Renee R. Frontiera*

Department of Chemistry, University of Minnesota

Minneapolis, MN 55455

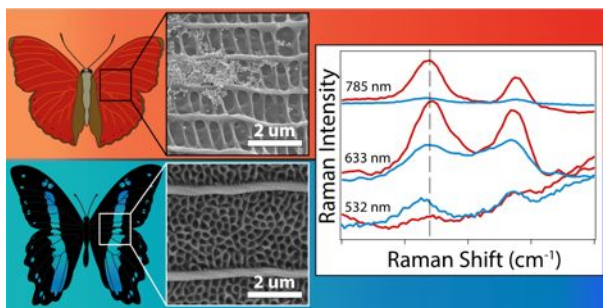
*To whom correspondence should be addressed. rrf@umn.edu, 612-624-2501

Abstract

Both plasmonic and photonic materials manipulate light by structurally-defined optical properties. While photonic architectures can promote the scattering and reflection of certain wavelengths of light, plasmonic materials have plasmon resonances that confine light at the nanoscale. Coupling photonic materials to plasmon resonances could enhance the plasmonic response via wavelength-dependent interference and confinement properties. Here we explore the use of wavelength-dependent, naturally-abundant photonic crystal structures found in butterfly wings as substrates for plasmonic nanoparticle deposition, and probe the plasmonic-photonic interactions using surface-enhanced Raman spectroscopy. To better understand the wavelength dependence of field enhancement and localization of these systems, we examined the SERS responses of plasmonic nanoparticles deposited on four different butterfly wing colors with three excitation wavelengths. We find that excitation at wavelengths most closely matching the butterfly wing color produces the most intense SERS signal, with signal magnitude increases up to an order of magnitude, beyond a mere additive effect. These naturally abundant photonic structures show potential to create

cheaper, wavelength-selective SERS substrates, and they provide a quantitative insight on plasmon-photonic crystal coupling.

TOC



The photonic architectures of butterfly wings selectively increase surface-enhanced Raman scattering and we quantitate the enhancement of this photonic-plasmonic interaction.

Introduction

Surface-enhanced Raman spectroscopy (SERS) can increase Raman signal magnitudes by factors up to 10^{12} , enabling single molecule detection of dozens of analytes.^{1, 2} SERS is primarily enabled by the field localization provided by the collective oscillation of conduction electrons on the surface of certain metals and semiconductors, also known as surface plasmon resonances. Upon excitation of a plasmon resonance, incident electromagnetic fields are concentrated to nanometer length scales, enabling strong enhancement of the Raman signal. SERS is highly sensitive to atomic scale changes in the size and shape of the supporting nanostructure.³ Designing the most sensitive SERS substrates with superior enhancement factors (EFs) is essential for the resolution of low intensity vibrations and small molecular concentrations of a wide range of analyte classes.

The signal amplification in SERS is most efficient in plasmonic hot spots, inclusive of geometries such as sharp points or small gaps between particles.⁴ These hot spots are known to dominate the SERS response, with the majority of the SERS signal coming from a very small portion of the nanomaterial surface.⁵ There is also a strong wavelength-dependence to SERS enhancement, with ensemble averaged measurements indicating that the maximum SERS signal occurs when the plasmon resonance maximum falls between the wavelengths of the Raman excitation laser and the Raman scattered signal.⁶ However, single particle results suggest that the EF depends more significantly on the substrate's efficacy at light confinement, rather than the LSPRs spectral location.⁷⁻⁹ Consideration of these factors is critical in the design of SERS measurements, and there has been significant effort in the development of new SERS substrates.⁴

Various plasmon-enhanced spectroscopic techniques incorporate dimerized structures¹⁰, lithographically-fabricated nanostars¹¹, metal films over nanospheres¹², and shell-isolated nanoparticles¹³ to improve spectroscopic detection of Raman scattering. In addition to colloidal and lithographic substrates, deposition of colloids onto structured surfaces has been quite promising for high signal magnitude, reproducible ensemble SERS measurements. The textured surface promotes nanoparticle aggregation and hot spot formation; and this effect has been successfully demonstrated for substrates such as filter paper¹⁴, rose petals¹⁵, and carbon nanotube networks¹⁶, among others. A particularly promising approach of integrating both photonic crystal architectures and plasmonic responses is to use naturally-abundant butterfly wing substrates to promote nanoparticle aggregation and field localization.¹⁷⁻²¹ However, previous studies do not probe both the photonic structure and plasmonic responses separately with different wavelengths of excitation, leading to a lack of quantitative understanding on the relationship of plasmonic and photonic coupling.

The butterfly wing's architecture produces its vibrant, often iridescent, structural colors from photonic crystal properties as well as absorption by pigment granules.²²⁻²⁵ Molecular subunits of chitin compose the cuticle which forms multiple quasi-periodic arrays on wing scales.^{17-19, 21, 23, 26-28} These photonic crystals within butterfly wings consist of periodic lamellae with branches of chitin (high refractive index) and gaps of air.²³ Incident light constructively interferes at a select wavelength defined by the photonic bandgap, as defined by each butterfly wing's periodic lamellae spacing.²³ We hypothesized that the butterfly wing's nanoscopic structure would promote nanoparticle aggregation and plasmonic hot spot formation, as well as providing wavelength-dependent enhancement due to constructive interference of the incident and Raman scattered fields. Several previous works have observed these coupling effects, and Tian et al. use experiment and theory to define the mechanism as coherent coupling between the plasmonic particles and the biophotonic structures.²⁹

Here, we use the naturally-occurring photonic structure found in butterfly wings as a substrate for plasmonic particle deposition. To determine the effect of coupling the butterfly's structural color to the plasmon resonances, we monitored the SERS intensity using a range of excitation wavelengths and butterfly wing colors. We find that matching the color of the wing to the excitation wavelength can in some instances increase the magnitude of the Raman scattering by a factor of ten, an impressive enhancement for a non-lithographic and naturally abundant photonic-plasmonic substrate. We compared changes in reflectance and SERS intensities, which supports the conclusion that plasmonic and photonic coupling has a beyond additive relationship. Therefore, aligning the plasmon excitation to the photonic bandgap of the butterfly wings results in a nonlinear increase in SERS signal enhancement.

Experimental Methods

Sample Preparation. We tested four different butterfly species, purchased from Butterfly Utopia: *Cymothoe sangaris* (red), *Eurema hecabe* (yellow), *Papilio bromius* (teal), and *Precis almana* (orange). We cut each butterfly wing to a 1 cm² area and adhered it to a glass slide with double-sided tape. Then we used a Technics Oxygen Asher Plasma Cleaner (150 sccm and 150 W for 35 seconds) to remove the hydrophobic wing coating in preparation for nanoparticle deposition.

We used colloidal silver nanoparticles and concentrated by centrifugation to approximately 3.1 x 10¹⁵ particles/L.^{30, 31} The nanoparticles had an average diameter of 101 nm as measured by electron microscopy (Figure S1). The extinction spectrum shows a monomer plasmon resonance peaked at 410 nm with a broad tail to the red indicative of a large heterogeneity in particle size and aggregation state, consistent with the electron microscopy imaging (Figure S1). We added MilliporeSigma pyridine (MilliporeSigma, Darmstadt, Germany) to the AgNP solution in a 50% volumetric concentration, and we deposited 10 μL of this 50% solution onto each 1 cm² region of butterfly wing (Fig. 1). For comparison, we also deposited the same solution onto a filter paper substrate, in which the texture of the fibers promotes nanoparticle aggregation and hot spot formation.

Surface-enhanced Raman Spectra. We collected all surface-enhanced Raman spectra using a home-built Raman setup. This design included an infinity-corrected objective (Olympus Ach 10X, 0.25) and a 30/70 beam splitter (CVI Laser) for collecting 180° geometrically-backscattered signal. The excitation sources were a 785 nm Innovative Photonic Solutions diode laser, a 633 nm ThorLabs HeNe laser, and a 532 nm Millenia VS laser, which provided 0.4 – 1 mW of power on the sample. We collected the Raman scattered signal with a Princeton Instruments PIXIS 100BX detector and Acton SpectraPro 2500i spectrograph. Our spectral acquisition times ranged from 0.1 – 1 s, depending on the scattering efficiency of the coupled butterfly wing-AgNP

system. We collected all spectra at normal incidence after aligning the laser to the marked center of the butterfly wing. We took four acquisitions at eight different locations on the wing, based on a consistent rectangular path around the wing center with 50 μm -spaced horizontal and 100 μm -spaced vertical probed locations (Fig. 2). We repeated all measurements with four different wing pieces from the same species in order provide representative spectra, which represent 128 spectra per substrate. We normalized all spectra with respect to excitation power and acquisition time to provide quantitative comparisons.

Data Analysis. We fit the 1008 cm^{-1} mode intensity with a Gaussian function on a linear baseline for each individual spectrum, and we used the intensity and standard deviation in the intensity for the values and errors in our analysis. We did find that structural heterogeneities arising from macroscopic features on the butterfly wings significantly impacted the SERS intensity and/or scattering background. These features include spots of significant color change, such as black portions of the wing, and ridges or veins of butterfly wing cuticle. As the photonic crystal properties in these regions were clearly impacted by these features, we excluded these regions from the overall data analysis.

Reflectance and Electron Microscopy Measurements. We measured the diffuse reflectance at normal incidence for each wing color and filter paper before and after AgNP-pyridine solution deposition using a Shimadzu UV-2600 UV-Vis spectrophotometer. We used a packed-powder diffusive plate reference and averaged three positions on each wing to generate the reported reflectance spectra. We collected scanning electron microscope images using a JEOL 6500 field emission gun SEM and a Focused Ion Beam (Dual-Beam FIB/SEM) (FIB) – FEI Helios G4 UX SEM.

Finite Element Method Simulation. To provide computational support to our wavelength-dependent SERS measurement interpretations, we simulated a AgNP dimer in a 1D photonic crystal with 2D finite element analysis using COMSOL Multiphysics Wave Optics Simulation Software (Version 5.4). The simulated cavity is $2 \times 2 \mu\text{m}$ with a 75 nm perfectly matched layer (PML) above and below the cavity, and periodic boundary conditions along the left and right edges. We defined the refractive indices for the 1D chitin photonic crystal³² and the AgNP dimer³³ based on previously reported values. We set the composition of the remaining volume as air. Our mesh has minimum and maximum dimensions of 1 nm and 30 nm, respectively. We varied the spacing between the photonic crystal layers (layers of 100 nm thickness) between 100, 150, and 200 nm to replicate the optical response of the different colored wings. We maintained a fixed nanoparticle radius of 50.5 nm, based on the average nanoparticle size in our experimental results, and included a dimer in the simulation to replicate the strong dependence of SERS signal magnitudes on hot spot formation. We used electromagnetic excitation of 1 W at normal incidence to the cavity ($\lambda = 300\text{--}900$ nm, 5 nm step), and we measured the cavity's integral reflectance across the boundary (normalized to the total excitation power) above the excitation port. We measured the reflectance observed for a AgNP dimer, three 1D chitin photonic crystals, and the AgNP dimer within each 1D chitin photonic crystal.

RESULTS AND DISCUSSION

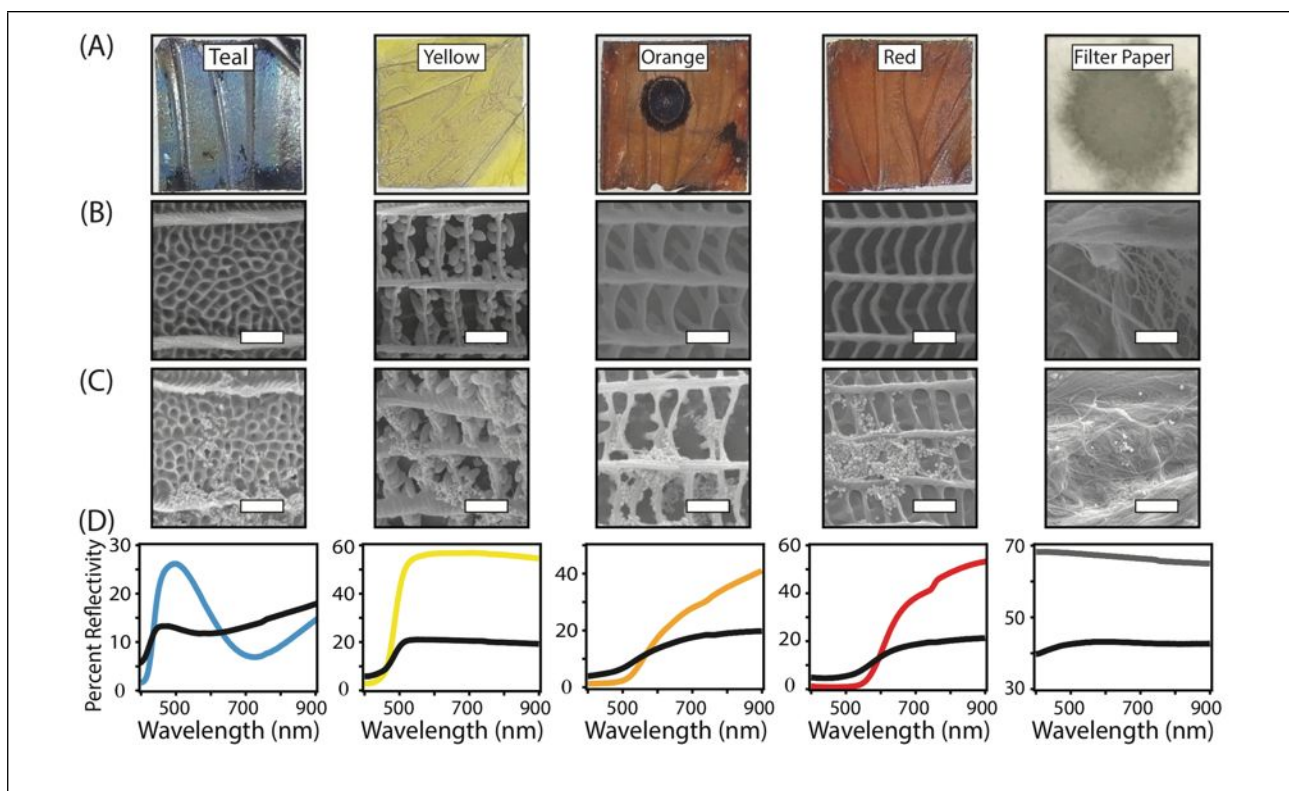
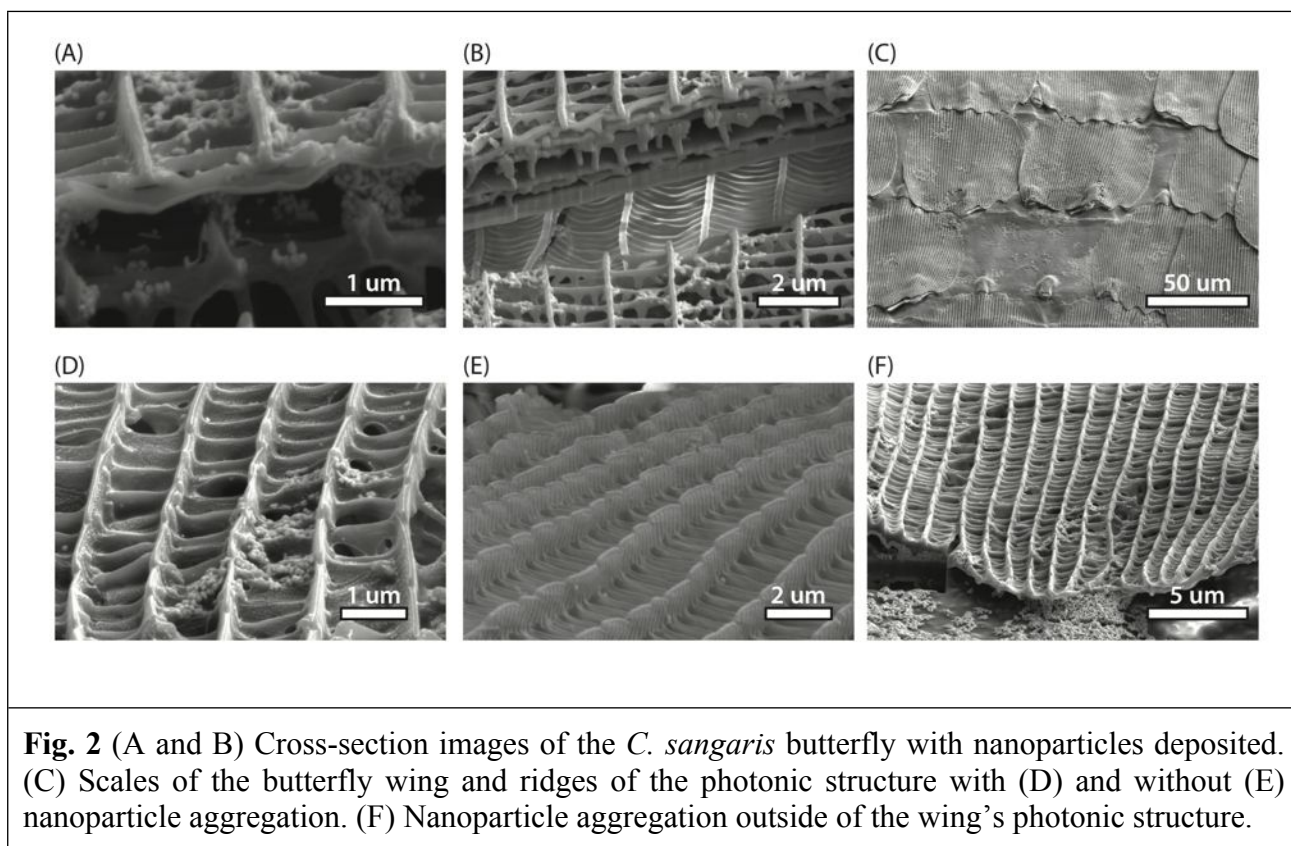


Fig. 1 (A) 1 cm² butterfly wing/filter paper substrates after depositing 10 μ L of a 50% silver nanoparticle-pyridine solution and the corresponding scanning electron micrographs before (B) and after (C) solution deposition. (D) Reflectance spectra for each sample. The scale bars in (B) are equivalent to 1 μ m. Spectral colors in (C) follow the color of the wing before (colored) and after (black) nanoparticle deposition.

We initially characterized the photonic-plasmonic structures through optical spectroscopy and electron microscopy. In Figure 1A, we show the optical images following nanoparticle deposition on the four butterfly wing types under examination, along with the filter paper control. We took care to keep the deposition area constant across all samples, although differences in the hydrophobicity of the various wing types as well as biological heterogeneities hindered rigorous uniformity, and thus we performed all measurements on a large number of samples. In Figure 1B and 1C we show SEM images of the wing structures before and after nanoparticle deposition, respectively. These images show characteristic horizontal ridges of micron-scale periodicity, as well as a sub-ridge foundation consisting of cross-ribs and trabeculae. In the red, orange, and

yellow wings these sub-ridge features are roughly rectangular, and in the teal wings the periodic webbing is circular.^{17, 27} These structures are consistent with previous SEM imaging on similar butterfly wings.^{17, 19, 21-23, 26-28, 34-38} As seen in Figure 1C, the nanoparticles adhere randomly to the wing structure, with large regions of aggregated nanoparticles. We confirmed that the wings retain their structural geometry after addition of the AgNP-pyridine solution, but we do observe some widening of the cross-rib webbing after comparing Figs. 1B and 1C. We also found, through cross-sectional SEM imaging, that the wing's structures consist of cuticular arrays in three-dimensions (Fig. 2), providing additional layers which also collected AgNP aggregates.



By measuring the diffuse reflectance of each wing, we assessed the wavelength-dependent scattering properties (Fig. 1D). The reflectance measurements prior to deposition (colored lines in Fig. 1D) show wavelength-dependent responses characteristic of the overall wing color. The filter

paper-nanoparticle control had reflectivity values of approximately 70% across the visible spectrum, due to the high diffusivity of this sample. Following deposition of silver nanoparticles, we observed significant damping of the reflectance in most of the butterfly wing samples, as shown in the black lines for each sample in Figure 1D, although the wavelength-dependent spectral features remained. We attribute increases in reflectivity after nanoparticle and pyridine deposition to the dissolution of pigments on the wings. Other spectral regions show increases in reflectivity, which suggests the addition of AgNPs hinders the photonic crystal optical properties. Butterfly wing photonic crystals consist of alternating layers of high (chitin) and low (air) refractive indices.³⁹ Filling spaces of air in the crystal with AgNPs increases the refractive index of the previously free spaces, with minimal impact to the overall structure. This is supported by our observation of the preservation of the underlying wing structure (Fig 1C and Fig 2) and the wavelength-dependent reflectance (Fig. 1D). Additionally, any signatures of the silver nanoparticle LSPR are minimal, primarily visible by an increase in the baseline around 450 nm, indicating that the dominant optical response arises from the photonic nature of the butterfly structure.

We hypothesized that we could increase the SERS signal magnitude through a constructive interference effect by matching the photoexcitation wavelength with the wing color. Previous works describe this effect as the coherent coupling of two resonant systems.^{29, 40, 41} Our wavelength-dependent methodology allows for a novel, quantitative measure of the relationship behind these coupling effects. We collected SERS spectra from all four wing types, as well as the filter paper control, using 532, 633, and 785 nm laser excitation. In Fig. 3 we show the averaged SER spectra of pyridine on the nanoparticle-wing substrates. The pyridine SER spectrum is dominated by modes at 1008 and 1035 cm^{-1} , corresponding to the ring breathing and C-C in-plane

bending modes, respectively. We observed some degree of SERS signal for all samples studied, with signal magnitudes ranging from 200 – 3000 cts/mW*s depending on the excitation wavelength and substrate. The filter paper control shows excellent SERS signal magnitudes for all excitation wavelengths, consistent with the nearly wavelength-independent reflectance spectra, as well as its use as a commercial SERS substrate.¹⁴ This is due to the highly heterogeneous and aggregating environment of the paper fibers. Interestingly, we see strong excitation wavelength dependent signal magnitudes for the different wing colors, which is most apparent through the large increase in signal magnitude for the orange and red wings using 785 nm excitation.

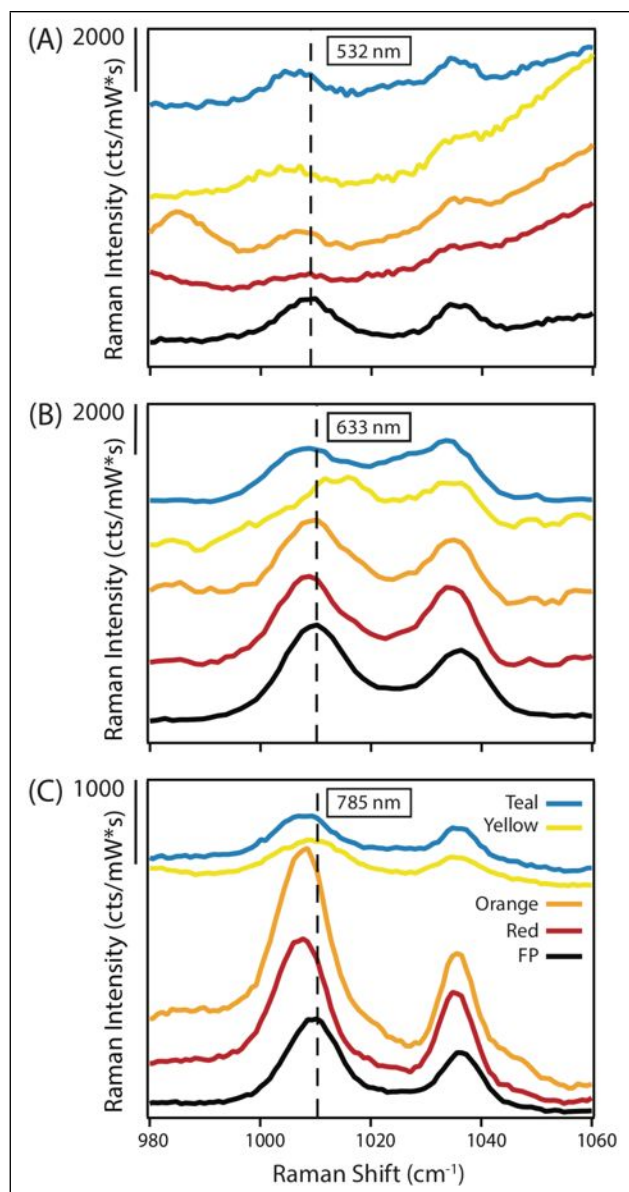


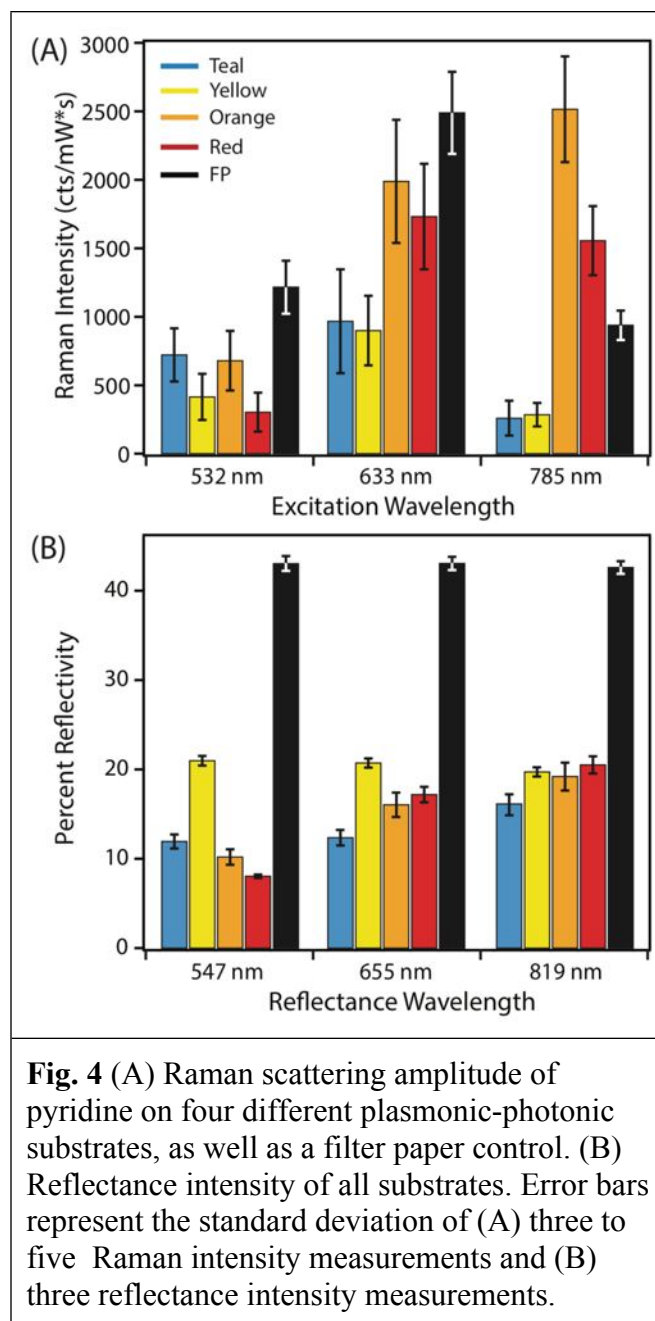
Fig. 3 Surface-enhanced Raman spectra of each butterfly wing at (A) 532 nm, (B) 633 nm, and (c) 785 nm laser excitation. Spectral colors correspond to the butterfly wing color, as denoted by the key in (C), along with the filter paper (FP) control.

To quantitate the impact of the wing photonic structure on the wavelength-dependent SERS signal magnitude, we fit the 1008 cm^{-1} peak in each averaged spectrum to a Gaussian lineshape and plotted the amplitudes in Fig. 4A. The error bars in Fig. 4A represent the average standard

deviation of the four butterfly wings' measured Raman intensity. The large magnitude of these errors bars likely results from the highly heterogenous butterfly wing topology and variable distribution of particle aggregation (as apparent in Fig. 2), which resulted in the relatively large standard deviation values for the filter paper control spectra. We see wavelength-dependent intensity trends for all samples, with evidence that suggests that matching the excitation wavelength to the wing color provides a more intense SERS response. For example, both the orange and the red wings show more intense signals at 633 nm and 785 nm excitation, as compared to 532 nm excitation. Looking at the reflectance spectra in Figure 1, it is clear that these wings have minimal optical response at 532 nm, and photonic crystal structures do not aid the SERS process at this wavelength. In contrast, the blue and yellow wings exhibit maximum SERS intensity with 532 nm and 633 nm excitation, with significantly reduced signal magnitude at 785 nm excitation. This is in agreement with the corresponding reflectivity spectra, which shows the onset of reflectance around 500 nm. It is important to note that reflectance results were influenced by pigmentation of the butterfly wings. Pigment granules were only apparent on SEM images of the yellow wings (Fig. 1C); but pigments were also present on the red, orange, and teal butterflies. To analyze the wing's pigments, we calculate differential reflectance spectra for unmodified butterfly wings and those bleached and with the AgNP/pyridine mixture (Fig. S4). The filter paper substrate provides remarkable SERS signal magnitudes at all excitation wavelengths, due to the ability of this highly textured substrate to promote nanoparticle aggregation leading to plasmonic hot spot formation.

A direct comparison of the structural color of the wing at the wavelength of excitation provides insight into the structural-plasmonic coupling relationship occurring within the wing. In Fig. 4B, we show the optical reflectance for each wing and the filter paper control. We report

values at wavelengths halfway between the laser excitation wavelength and the Raman scattering wavelength for each of the three laser sources used. This average wavelength accounts for both of the frequencies involved in the Raman process. There is qualitative agreement between the wavelength trends of SERS signal magnitude and reflectivity across each wing color. For example, the red and orange wings exhibit lowered reflectivity at 547 nm as compared to 655 nm and 819 nm, in agreement with the increased SERS signals with red and near infrared excitation. A more quantitative relationship between the photonic structure and coupled plasmonic response is hindered by competing optical processes, namely resonant scattering effects from hybridized plasmon modes in aggregated nanoparticles, and absorption by wing pigments. However, we show through wing bleaching experiments that pigments only effect, at most, the optical absorption at one excitation wavelength for all but the teal wings (Fig. S4). We then use the filter paper as a reference for the LSPR aggregation effects in order to quantify the wavelength-dependent photonic-plasmonic coupling.



We remove the wavelength-dependent nanoparticle aggregate LSPR and Raman scattering cross section from our results by normalizing all Raman and reflectance intensities to those measured on filter paper (Fig. 5), which to first approximation should account for all plasmon effects as the particles are similarly aggregated and ensemble-averaged. This normalization allows for interpretation of the wavelength-dependent photonic-plasmonic coupling without impacts from

the wavelength-dependent LSPR or Raman scattering cross section because these effects are contained in the filter paper SERS spectra. Therefore, the normalized results primarily include wavelength-dependent responses occurring due to plasmonic and photonic coupling. To quantify the magnitude of this wavelength-dependent coupling, we calculated the differences between the Raman scattering ratios (Fig. 5A) and reflectivity ratios (Fig. 5B) at 633 and 785 nm from 532 nm excitation wavelengths (Fig. 5B). We use the reflectance difference measurements at the wavelength of the Raman scattered light to show the influence of the photonic structure's optical properties which produce the observed excitation wavelength-dependent response in the SERS results.

Both linear and nonlinear effects have been reported for light interactions within biophotonic materials, but the effects of photonic and plasmonic coupling have yet to be defined experimentally.³⁹ Here, Figs. 5B and 5D describe the relationship between photonic structure and the plasmonic response, which shows that the magnitude of the SERS signal increase is not a merely additive effect. Comparing the trend in the data of Fig. 5D to that in Fig. 5B supports this conclusion because aligning the excitation wavelength to the optical properties of the photonic structure results in a nonlinear response in the SERS data. For example, the red butterfly wing has increased reflectance ratio differences of 0.21 ± 0.04 and 0.30 ± 0.05 for 655 - 547 nm and 819 - 547 nm, respectively. The corresponding Raman ratio differences are 0.45 ± 0.21 and 1.41 ± 0.35 for 633-532 nm and 785-532 nm, respectively. It is apparent that changes in the SERS response are much greater than those for the reflectance measurements at the wavelengths of interest, particular in the NIR excitation region. An identical effect is observed with the orange butterfly wings when comparing the optical responses with the filter paper control. The reflectance ratio differences are 0.14 ± 0.08 for 655 - 547 nm and 0.21 ± 0.09 for 819 - 547 nm. The corresponding

Raman ratio differences are 0.24 ± 0.29 and 2.12 ± 0.55 for 633 – 532 nm excitation and 785 – 532 nm excitation, respectively. Thus, for both the red and the orange wings, the increase in the SERS signal does not increase linearly with the reflectance response. Conversely, the teal butterfly wings do not experience coupling at larger wavelengths as their Raman scattering magnitude decreases with wavelength. The yellow wings do not preferentially couple to any one excitation wavelength because neither their photonic nor SERS response changes in the relevant visible region. The mechanism behind this coupling is referenced as a coherent coupling effect between the resonant systems of the plasmonic AgNPs and the photonic lattice.²⁹ Coherent coupling is also well supported by previous theoretical calculations.^{18, 26, 29} However, our work is the first to use wavelength-dependent SERS measurements to highlight the relationship of coupling, and it does not explicitly report on the mechanism responsible. Similar studies could also integrate a wavelength-dependent SERS probe to investigate the near-field coupling relationship in metal/semiconductor interfaces or catalytic heterostructures.

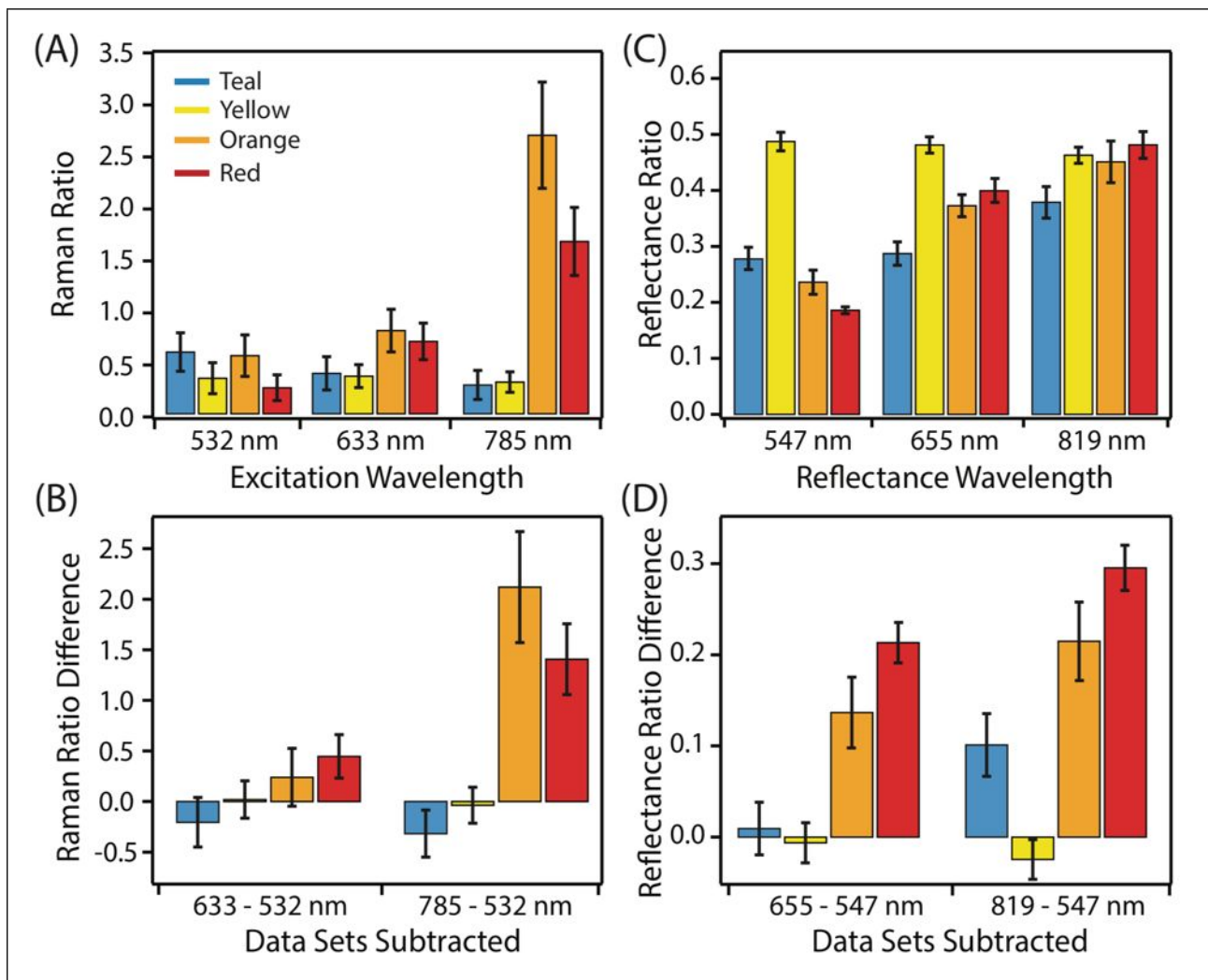


Fig. 5 (A) Results from Fig. 4A normalized to the filter paper reference from each data set and (B) subtracted to show changes in Raman intensity of 633 and 785 nm from 532 nm excitation. (C) and (D) Identical calculations as (A) and (B) for results from Fig. 4B. All bar colors follow the legend in (A). Error bars correspond to the propagated error from (B) 3-5 Raman intensity and (D) 3 reflectance measurements.

To simulate the coupling of plasmonic nanoparticles with the butterfly wing's photonic crystal, we implemented finite element analysis using 2D COMSOL Multiphysics Wave Optics Simulation Software. Fig. 6 depicts a 1 W EM field scattered by a 1D photonic crystal (100, 150, and 200 nm gap between chitin layers) and a AgNP dimer on a photonic crystal. We present our theoretical results for the three wavelengths of excitation which match the experimental Raman

excitation wavelengths (530, 635, and 785 nm). We simulated the wavelength-dependent reflectance of the AgNP-photonic crystal system for three gap sizes, approximating different color butterfly wings. As expected, there is a complex field interaction between the AgNPs with high optical cross section and the periodic photonic crystal. These interactions are strongest when the resonant wavelength of the photonic crystal matches the excitation wavelength.

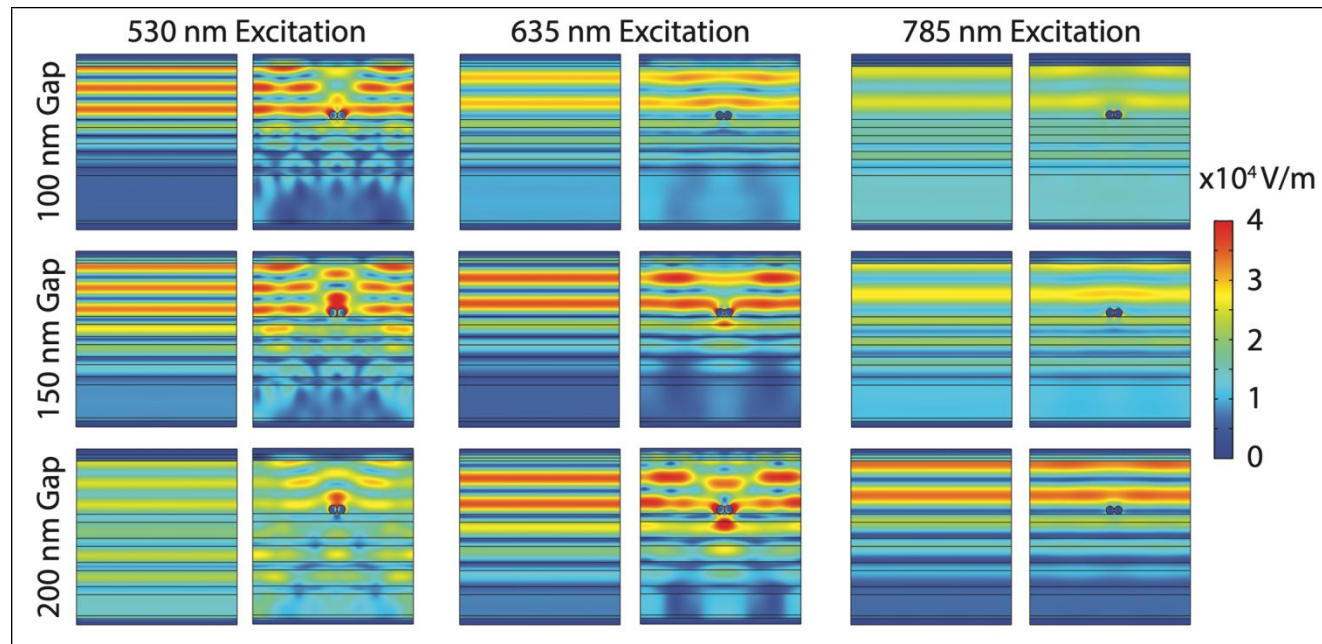


Fig. 6 An EM field simulation after interaction with a chitin photonic crystal and a silver nanoparticle dimer-photonic crystal system at three wavelengths of excitation and three photonic crystal layer periodicities. For each excitation condition, the left column shows the field interaction with the photonic crystal alone, and the right column shows the field interaction with the AgNP-photonic crystal.

To analyze the magnitude of plasmonic-photonic coupling, we separately simulated the reflectance of a AgNP dimer and of each 1D photonic crystal. We tested our experimental result by adding and multiplying the reflectance spectra from the AgNP dimer and each photonic crystal to measure the coupling intensity. Then, we compared the reflectance spectra of the AgNP-photonic crystal system to the sum and the product of the reflectance spectra for a AgNP dimer and a photonic crystal. We found that adding the spectra better matches the reflectance produced

by the combined AgNP-photonic crystal system (Fig. 7). However, the added spectra fail to match the AgNP-photonic crystal reflectance at the peak reflectance intensities of the photonic crystal. The difference in reflectance intensity is likely the result of additional AgNP absorption generated by coupling to the photonic crystal, further supporting the previously proposed coupling mechanism. Our theoretical results present the beyond-additive effects of photonic and plasmonic coupling and support our experimental conclusion.

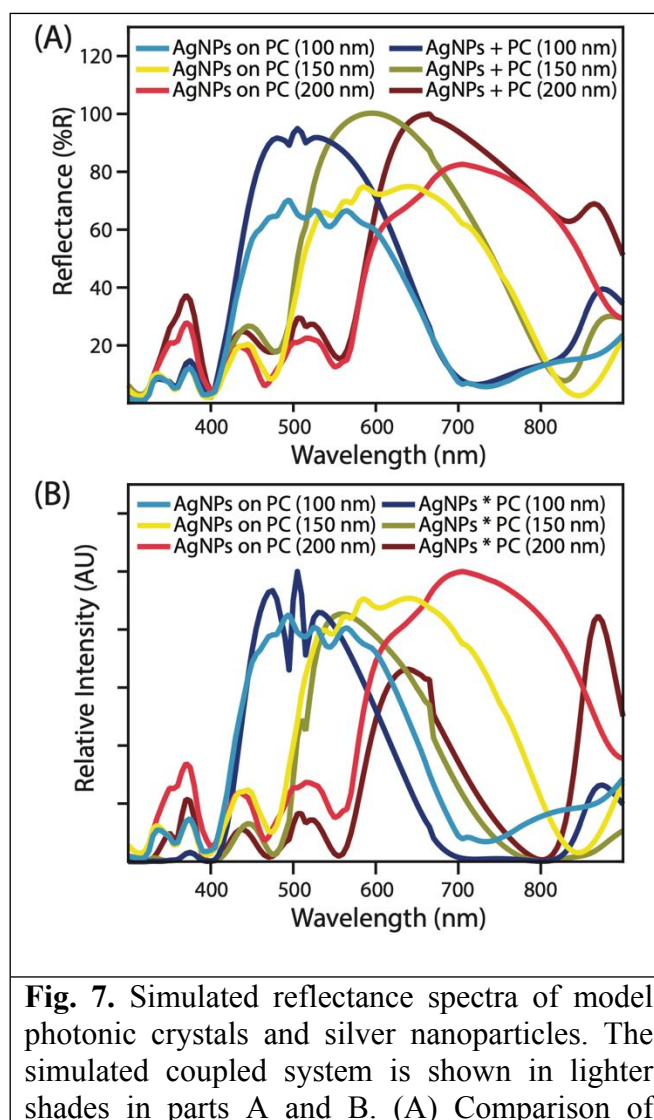


Fig. 7. Simulated reflectance spectra of model photonic crystals and silver nanoparticles. The simulated coupled system is shown in lighter shades in parts A and B. (A) Comparison of

coupled response to summation of individual photonic crystal and AgNP spectra. (B) Comparison of the coupled response to the multiplication of individual photonic crystal and AgNP spectra.

CONCLUSIONS

In this work, we have found that using the natural photonic structures of butterfly wings can promote wavelength-selective increases in SERS scattering. By matching the color of the wing to the excitation wavelength we can, in some instances, increase the magnitude of the Raman scattering by nearly an order of magnitude above the wavelength-mismatched measurements, despite the heterogeneous nature of the substrates. We are the first to describe the nonlinear relationship of coupling effects between plasmonic and photonic nanostructures using a wavelength-dependent SERS probe. The non-lithographic and naturally abundant photonic crystals found in butterfly wings provide a substrate for nanoparticle deposition and aggregation and enable this increased SERS response. Further increases in SERS signal will likely require more homogeneous, wavelength-dependent photonic crystal structures which could be incorporated as spectrally-selective or multiplexed SERS substrates.⁴²⁻⁴⁴ However, the ease of fabrication and low cost of the photonic-plasmonic substrates described here should provide a significant advantage for facile wavelength-dependent SERS measurements.

CONFLICTS OF INTEREST

There are no conflicts to declare.

ACKNOWLEDGEMENTS

We thank Dayeeta Saha, Christopher Warkentin, and Emily Keller for SEM characterization. We also thank Matthew Yang who performed measurements which preceded this work. This work was supported by the Air Force Office of Scientific Research under AFOSR award no. FA9550-15-1-0022 and the University of Minnesota Undergraduate Research Opportunities Program. Parts of this work were carried out in the Characterization Facility at the University of Minnesota, which receives partial support from the NSF through the MRSEC program (DMR-1420013). The authors acknowledge the Minnesota Supercomputing Institute (MSI) at the University of Minnesota for providing resources that contributed to the research results reported within this paper.

Supporting Information Available: Additional experimental method information, scanning electron micrographs, Raman spectral characterization, and COMSOL Multiphysics Wave Optics simulation results.

REFERENCES

1. P. L. Stiles, J. A. Dieringer, N. C. Shah and R. P. Van Duyne, *Annu Rev Anal Chem*, 2008, **1**, 601-626.
2. K. Kneipp, Y. Wang, H. Kneipp, L. T. Perelman, I. Itzkan, R. Dasari and M. S. Feld, *Phys Rev Lett*, 1997, **78**, 1667-1670.
3. S. Lal, S. Link and N. J. Halas, *Nat Photonics*, 2007, **1**, 641-648.
4. S. L. Kleinman, R. R. Frontiera, A. I. Henry, J. A. Dieringer and R. P. Van Duyne, *Phys Chem Chem Phys*, 2013, **15**, 21-36.
5. Y. Fang, N. H. Seong and D. D. Dlott, *Science*, 2008, **321**, 388-392.
6. K. A. Willets and R. P. Van Duyne, *Annu Rev Phys Chem*, 2007, **58**, 267-297.
7. S. L. Kleinman, B. Sharma, M. G. Blaber, A. I. Henry, N. Valley, R. G. Freeman, M. J. Natan, G. C. Schatz and R. P. Van Duyne, *J Am Chem Soc*, 2013, **135**, 301-308.
8. A. M. N. Michaels, M.; Brus, L.E., *J Am Chem Soc*, 1999, **121**, 9932-9939.
9. K. Hoflich, U. Gosele and S. Christiansen, *J Chem Phys*, 2009, **131**, 164704.
10. P. H. Camargo, L. Au, M. Rycenga, W. Li and Y. Xia, *Chem Phys Lett*, 2010, **484**, 304-308.
11. M. Chirumamilla, A. Toma, A. Gopalakrishnan, G. Das, R. P. Zaccaria, R. Krahne, E. Rondanina, M. Leoncini, C. Liberale, F. De Angelis and E. Di Fabrizio, *Adv Mater*, 2014, **26**, 2353-2358.

12. J. L. Brooks and R. R. Frontiera, *J Phys Chem C*, 2016, **120**, 20869-20876.
13. J. F. Li, Y. F. Huang, Y. Ding, Z. L. Yang, S. B. Li, X. S. Zhou, F. R. Fan, W. Zhang, Z. Y. Zhou, D. Y. Wu, B. Ren, Z. L. Wang and Z. Q. Tian, *Nature*, 2010, **464**, 392-395.
14. Ocean Optics SERS Substrates, <https://oceanoptics.com/product/sers/>, (accessed May 1, 2019).
15. S. Y. Chou, C. C. Yu, Y. T. Yen, K. T. Lin, H. L. Chen and W. F. Su, *Anal Chem*, 2015, **87**, 6017-6024.
16. Y. C. Chen, R. J. Young, J. V. Macpherson and N. R. Wilson, *J Phys Chem C*, 2007, **111**, 16167-16173.
17. N. L. Garrett, P. Vukusic, F. Ogrin, E. Sirotkin, C. P. Winlove and J. Moger, *J Biophotonics*, 2009, **2**, 157-166.
18. X. Y. Yan, Y. H. Wang, G. C. Shi, M. L. Wang, J. Z. Zhang, X. Sun and H. J. Xu, *Optik*, 2018, **172**, 812-821.
19. J. He, Q. Shen, S. Yang, G. He, P. Tao, C. Song, J. Wu, T. Deng and W. Shang, *Nanoscale*, 2018, **10**, 533-537.
20. C. C. Fu, Y. J. Gu, Z. Y. Wu, Y. Y. Wang, S. P. Xu and W. Q. Xu, *Sensor Actuat B-Chem*, 2014, **201**, 173-176.
21. Y. Tan, X. Zang, J. Gu, D. Liu, S. Zhu, H. Su, C. Feng, Q. Liu, W. M. Lau, W. J. Moon and D. Zhang, *Langmuir*, 2011, **27**, 11742-11746.
22. Y. Ding, S. Xu and Z. L. Wang, *J Appl Phys*, 2009, **106**.
23. S. Kinoshita and S. Yoshioka, *Chemphyschem*, 2005, **6**, 1442-1459.
24. H. Ghiradella, *J Morphol*, 1989, **202**, 69-88.
25. H. Ghiradella, *Appl Opt*, 1991, **30**, 3492-3500.
26. R. Yan, M. Chen, H. Zhou, T. Liu, X. Tang, K. Zhang, H. Zhu, J. Ye, D. Zhang and T. Fan, *Sci Rep*, 2016, **6**, 20001.
27. B. D. Wilts, T. M. Trzeciak, P. Vukusic and D. G. Stavenga, *J Exp Biol*, 2012, **215**, 796-805.
28. Z. D. Mu, X. W. Zhao, Z. Y. Xie, Y. J. Zhao, Q. F. Zhong, L. Bo and Z. Z. Gu, *J Mater Chem B*, 2013, **1**, 1607-1613.
29. J. Tian, W. Zhang, X. Fang, Q. Liu, J. Gu, T. Deng, Y. Wang and D. Zhang, *J Mater Chem C*, 2015, **3**, 1672-1679.
30. P. C. Lee and D. Meisel, *J Phys Chem*, 1982, **86**, 3391-3395.
31. W. Meng, F. Hu, X. Jiang and L. Lu, *Nanoscale Res Lett*, 2015, **10**, 34.
32. D. E. Azofeifa, H. J. Arguedas and W. E. Vargas, *Opt Mater*, 2012, **35**, 175-183.
33. P. B. Johnson and R. W. Christy, *Phys Rev B*, 1972, **6**, 4370-4379.
34. S. G. Romanov, A. S. Susa, C. M. S. Torres, Z. Liang and F. Caruso, *J Appl Phys*, 2005, **97**, 086103.
35. S. Panettieri, E. Gjinaj, G. John and D. J. Lohman, *PLoS One*, 2018, **13**, e0202465.
36. G. S. Smith, *Am J Phys*, 2009, **77**, 1010-1019.
37. D. J. Kemp, *Behav Ecol*, 2008, **19**, 1-8.
38. R. T. Lee and G. S. Smith, *Appl Opt*, 2009, **48**, 4177-4190.
39. C. Verstraete, S. R. Mouchet, T. Verbiest and B. Kolaric, *J Biophotonics*, 2019, **12**, e201800262.
40. Z. C. Ye, S.; Kuang, P.; Ho, K.-M., *Opt Express*, 2012, **20**, 12213-12221.
41. F. Le, D. W. Brandl, Y. A. Urzhumov, H. Wang, J. Kundu, N. J. Halas, J. Aizpurua and P. Nordlander, *ACS Nano*, 2008, **2**, 707-718.

42. L. Sun, H. Lin, K. L. Kohlstedt, G. C. Schatz and C. A. Mirkin, *Proc Natl Acad Sci U S A*, 2018, **115**, 7242-7247.
43. X. Y. Zhou and N. M. Kostic, *Inorg Chem*, 1988, **27**, 4402-4408.
44. C.-G. Chae, Y.-G. Yu, H.-B. Seo, M.-J. Kim, R. H. Grubbs and J.-S. Lee, *Macromolecules*, 2018, **51**, 3458-3466.

